J. Fluid Mech. (1988), *vol.* 197, *pp.* 331–348
Printed in Great Britain

Finite-amplitude evolution of two-layer geostrophic vortices

By KARL R. HELFRICH† AND UWE SEND‡

† Woods Hole Oceanographic Institution, Woods Hole, MA 02543, USA

‡ Scripps Institution of Oceanography, La Jolla, CA 92093, USA

(Received 11 December 1987 and in revised form 28 March 1988)

The finite-amplitude evolution of circular two-layer quasi-geostrophic vortices with piecewise uniform potential vorticity in each layer (also termed 'heton' clouds by Hogg & Stommel 1985*a* and Pedlosky 1985) is studied using the contour dynamics method. The numerical investigations are preceded by a linear stability analysis which shows the stabilizing influence of deepening the lower layer. Net barotropic flow may be either stabilizing or destabilizing. The contour dynamics calculations for baroclinic vortices show that supercritical (i.e. linearly unstable) conditions may lead to explosive break up of the vortex via the generation of continuous hetons at the cloud boundary. The number of vortex pairs is equal to the azimuthal mode number of the initial disturbance. An additional weakly supercritical regime in which amplitude vacillation occurs, but not explosive growth, is identified. Vortices with net barotropic circulation behave similarly except that the layer with vorticity opposite to the barotropic circulation will break up first. Strong barotropic circulation can inhibit the development of hetons. The stronger layer may eject thin filaments, but remain mostly intact. Calculations for initial conditions composed of several unstable modes show that the linearly most unstable mode dominates at finite amplitude.

1. Introduction

Hogg & Stommel (1985*b*) investigated the interactions of point vortices in a two-layer quasi-geostrophic f-plane system. A novel feature of these baroclinic vortex interactions was the existence of vortex pairs which could transport heat – 'hetons'. A heton consists of two point vortices, of opposite signs in opposite layers, which are laterally offset. Mutual advection leads to propagation in a direction perpendicular to the line connecting the centres if the strengths and layer depths are equal. Non-equal layer depths or strengths causes curved paths. The baroclinic structure permitted net heat transport. Hogg & Stommel (1985*b*) and Young (1985) further investigated the interactions of two hetons and found a range of behaviours from coalescence to repulsion, depending on the signs, strengths and initial separation of the individual hetons.

In an effort to explain the break up of warm pools of water Hogg & Stommel (1985*a*) extended the vortex interaction studies to consider large assemblages (or clouds) of point vortices in a two-layer system with equal depths, H_1. They found that a circular baroclinic heton cloud of radius L (unit strength positive vortices in the upper layer and unit strength negative vortices in the lower layer for radius $r \leqslant L$) would break up into m composite hetons. These smaller heton clouds would then propagate radially outward. The number of composite hetons was found empirically

to be given by $m = 1.10F_1$ for $m \geqslant 2$, where $F_1 = f^2L^2/g'H_1$, L is the initial cloud radius, g' is the reduced gravity and f is the Coriolis frequency. The internal rotational Froude number F_1 is a measure of the eddy radius compared with the internal Rossby deformation radius $\lambda = (\frac{1}{2}g'H_1)^{\frac{1}{2}}f^{-1}$.

Pedlosky (1985) examined the linear stability of the continuous version of the circular heton cloud. For equal layer depths and equal and opposite potential vorticities in the upper and lower layers of a cloud of radius L the cloud was found to be unstable to longwave disturbances. For large cloud radii $m \sim 2^{\frac{1}{2}}F_1$. The instability occurred when perturbations of the upper and lower cloud boundaries were appropriately out of phase. Mutual interaction between the layers resulted in growth of the disturbance. The boundary perturbations can be thought of as acting like single point vortices. The phase difference between layers is analogous to the lateral offset necessary for heton self-propulsion and the arrangement is such that vortex pairs will propagate radially outward. Pedlosky (1985) further considered the linear and weakly nonlinear behaviour of a straight cloud band. The linear analysis exhibited the same type of instability as the circular geometry. The nonlinear analysis required the supercriticality $\Delta \equiv (F_1 - F_{1c})/F_{1c} \ll 1$, where F_{1c} is the value of F_1 at the linear stability boundary. Pedlosky showed that interaction of the fundamental wave with its next higher harmonic resulted in explosive growth for all unstable wavenumbers. These results were consistent with the point vortex model of Hogg & Stommel (1985*a*).

In this paper we generalize the linear stability analysis and present numerical studies of the continuous two-layer f-plane baroclinic vortex instability at finite amplitude. This is accomplished via the contour dynamics method (Zabusky, Hughes & Roberts 1979) which we have formulated for multilayer quasi-geostrophic systems. The method allows the fully nonlinear evolution to be followed with the requirement that the system consists of regions of uniform potential vorticity.

In a related study Ikeda (1981) examined the linear and nonlinear evolution of a circular baroclinic eddy in a two-layer quasi-geostrophic f-plane system. The eddies had a nearly Gaussian profile of potential vorticity in each layer rather than a piecewise uniform distribution. For the particular geometry and vorticity distributions studied he found that the vortex was most unstable to a mode 2 azimuthal disturbance. Finite-amplitude evolution for unstable mode 2 disturbances showed initial eddy elongation followed by either return to a circular eddy for small linear growth rates or splitting of the eddy into two smaller eddies for larger growth rates.

Ikeda's results are similar to Hogg & Stommel (1985*a*) and Pedlosky (1985) in that instability may lead to break up of the eddy, but differ in the fact that some cases lead to a return to a circular eddy. Although our proposed model requires piecewise uniform potential vorticity, it does allow for full nonlinear development of the instability. As such, it contains the full nonlinearity of Ikeda's calculations and the simple vorticity distribution of the heton cloud studies while retaining more resolution than the point vortex model. Thus it should help to unify the earlier results. Indeed, we find both vacillation and explosive regimes analogous to Ikeda's calculations.

The paper is organized as follows. In §2 the linear theory is extended to examine the effects of unequal layer depths and net barotropic flow on stability. In §3 the contour dynamics formulation for two active layers on an f-plane is presented. Numerical results appear in §4, followed by a discussion of the results in §5.

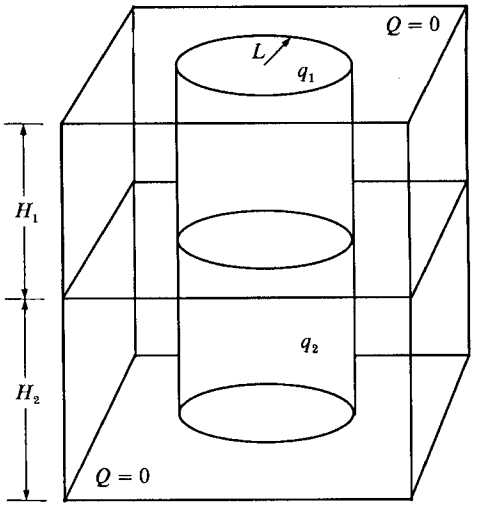

FIGURE 1. Definition sketch for the two-layer circular vortex.

During the final preparation of this paper we became aware of some recent work by Kozlov, Makarov & Sokolovskiy (1986) which anticipates some of the results of this work. They formulate a similar contour dynamics problem but only examine the finite-amplitude evolution for one example. Our work covers aspects which are not addressed there, such as evolution with net barotropic circulation and evolution with several unstable modes in the initial condition. Furthermore, we find vacillating behaviour.

2. Linear stability analysis

In this section the linear stability of a circular two-layer quasi-geostrophic vortex on the f-plane is examined. The derivation follows the analysis of Pedlosky(1985) with the addition of unequal layer depths and net barotropic circulation. This linear stability analysis serves as background to the finite-amplitude calculations discussed in §4.

Consider the two-layer system in which the quasi-geostrophic potential vorticity in layer n,

$$Q_n = \nabla^2\psi_n + (-1)^n F_n(\psi_1 - \psi_2), \tag{2.1}$$

is a constant, q_n, for $r \leqslant 1$ and zero for $r > 1$ (see figure 1). The conservation of potential vorticity in each layer requires

$$\left\{\frac{\partial}{\partial t} - \frac{\partial\psi_n}{\partial y}\frac{\partial}{\partial x} + \frac{\partial\psi_n}{\partial x}\frac{\partial}{\partial y}\right\} Q_n = 0. \tag{2.2}$$

Here ψ_n is the stream function in layer $n = 1, 2$ (upper and lower layers respectively) and $F_n = L^2f^2/g'H_n$ is the rotational Froude number in layer n. H_n is the undisturbed depth in layer n, f is the Coriolis frequency and $g' = g(\rho_2 - \rho_1)/\rho_0$ is the reduced gravity. Here (2.1) and (2.2) have been normalized by the eddy radius L, a velocity scale U, the timescale L/U and the potential vorticity scale U/L.

The basic steady state stream function, $\Psi_n(r)$, is obtained by solving (2.1) for the

potential vorticity distribution in figure 1 with the conditions that Ψ_n is regular at $r = 0, \infty$ and Ψ_n and $\partial\Psi_n/\partial r$ are continuous at $r = 1$. This gives

$$\Psi_n = (1+\delta)^{-1} \begin{cases} \frac{1}{4}\delta q_B(r^2-1) + (-\delta)^{n-1} q_T k^{-2}(1 - kK_1(k) I_0(kr)) & (r \leqslant 1), \\ \frac{1}{2}\delta q_B \log r + (-\delta)^{n-1} q_T k^{-1} I_1(k) K_0(kr) & (r > 1), \end{cases} \tag{2.3}$$

where $$q_B = q_1 + \delta^{-1} q_2, \quad q_T = q_1 - q_2, \quad k = (F_1+F_2)^{\frac{1}{2}}, \tag{2.4a–c}$$

and $$\delta = H_1/H_2 = F_2/F_1. \tag{2.4d}$$

Here q_B and q_T are the barotropic and baroclinic potential vorticities, respectively, and K_m and I_m are modified Bessel functions of order m. From (2.3) the basic-state azimuthal velocities, $V_n(r) = \partial\Psi_n/\partial r$, are

$$V_n(r) = (1+\delta)^{-1} \begin{cases} \delta q_B \tfrac{1}{2} r + (-\delta)^{n-1} q_T K_1(k) I_1(kr) & (r \leqslant 1), \\ \delta q_B \tfrac{1}{2} r^{-1} + (-\delta)^{n-1} q_T I_1(k) K_1(kr) & (r > 1). \end{cases} \tag{2.5}$$

Within each uniform potential vorticity region linear perturbations, $\phi_n(r, \theta, t)$, to the basic state must satisfy

$$\nabla^2 \phi_n + F_n(-1)^n (\phi_1 - \phi_2) = 0, \tag{2.6}$$

along with the boundary conditions (Pedlosky 1985)

$$\phi_n \quad \text{regular at } r = 0, \infty, \tag{2.7a}$$

$$\phi_n \quad \text{continuous at } r = 1, \tag{2.7b}$$

and $$\left(\frac{\partial}{\partial t} + \frac{V_n}{r}\frac{\partial}{\partial \theta}\right)\frac{\partial \phi_n}{\partial r} - \frac{1}{r}\frac{\partial \phi_n}{\partial \theta}\frac{\mathrm{d}V_n}{\mathrm{d}r} \quad \text{continuous at } r = 1. \tag{2.7c}$$

The last of these is a statement of pressure continuity at the boundary. Searching for normal mode solutions of the form

$$\phi_n = \Phi_n(r)\, \mathrm{e}^{\mathrm{i}(m\theta - \omega t)}, \tag{2.8}$$

where m is the azimuthal wavenumber and ω is the complex frequency, the boundary conditions (2.7a, b) give

$$\Phi_n(r) = \begin{cases} Ar^m + B(-\delta)^{n-1} I_m(kr)/I_m(k) & (r \leqslant 1), \\ Ar^{-m} + B(-\delta)^{n-1} K_m(kr)/K_m(k) & (r > 1). \end{cases} \tag{2.9}$$

From the dynamic boundary condition (2.7c), two equations for A and B are found,

$$A[2\delta m(V_1(1)\, m - \omega) - m\delta q_1] + B\left[\frac{V_1(1)\, m - \omega}{I_m(k) K_m(k)} - m q_1\right] = 0, \tag{2.10a}$$

and $$A[2m(V_2(1)\, m - \omega) - m q_2] + B\left[\frac{-(V_2(1)\, m - \omega)}{I_m(k) K_m(k)} + m q_2\right] = 0. \tag{2.10b}$$

$V_n(1)$ refers to the velocity in layer n at $r = 1$ from (2.5). For non-trivial solutions the

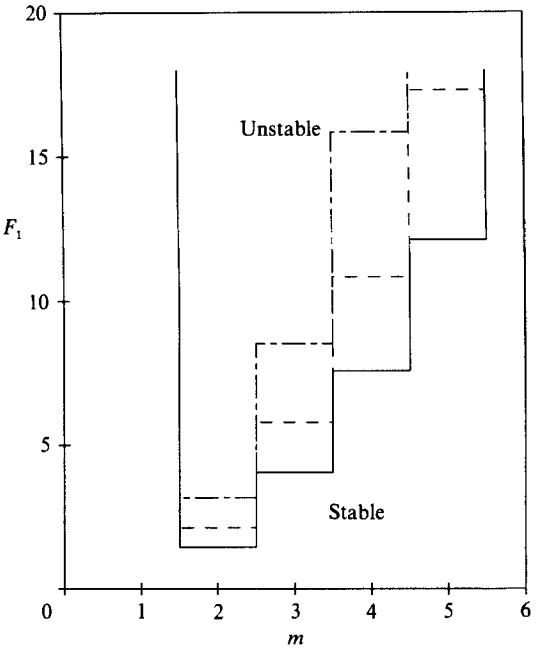

FIGURE 2. Stability diagram for the purely baroclinic case, $q_B = 0$ and several layer depth ratios: ——, $\delta = 1$; – – –, $\delta = 0.5$; –·–·–, $\delta = 0.25$.

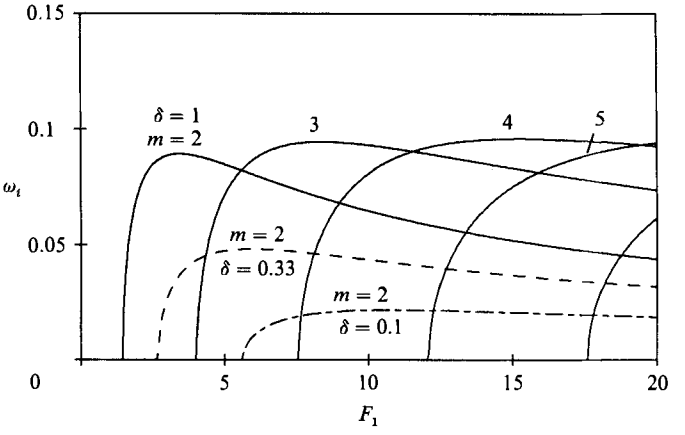

FIGURE 3. Growth rates, ω_i, for the purely baroclinic vortex, $q_B = 0$, as a function of F_1: ——, $\delta = 1.0$ and $m = 2$–6; – – –, $\delta = 0.33$ and $m = 2$; –·–·–, $\delta = 0.1$ and $m = 2$.

determinant of the coefficients in (2.10) must be zero, which leads to the dispersion relationship for $c = \omega/m$,

$$c^2\{-2m(1+\delta)\}+c\{(1+\delta)\,2m(V_1(1)+V_2(1))-2mK_m(k)\,I_m(k)\,(q_1+\delta q_2)$$
$$-(\delta q_1+q_2)\}+\{-2m(1+\delta)\,V_1(1)\,V_2(1)+2mK_m(k)\,I_m(k)\,(\delta q_2\,V_1(1)+q_1\,V_2(1))$$
$$+(\delta q_1\,V_2(1)+q_2\,V_1(1))-q_1\,q_2K_m(k)\,I_m(k)\,(1+\delta)\}=0. \quad (2.11)$$

When $\delta = 1$ and $q_B = 0$ (2.11) reduces to (3.10) in Pedlosky (1985).

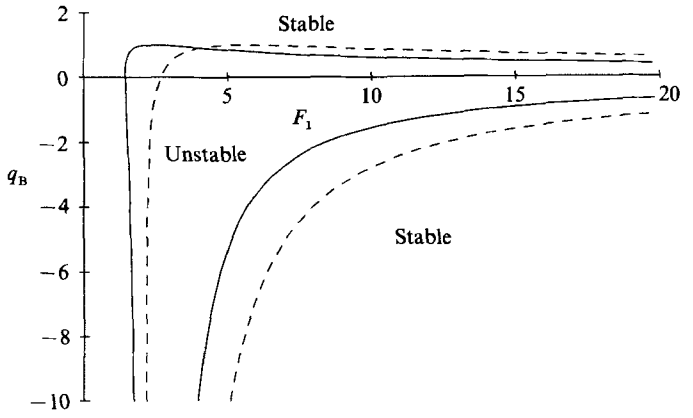

FIGURE 4. Stability diagram for net barotropic circulation with $m = 2$ and $q_1 = 1$: ——, $\delta = 1$; – – –, $\delta = 0.33$.

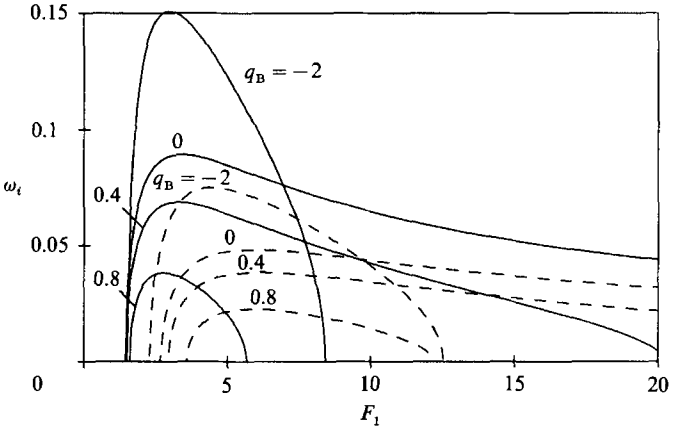

FIGURE 5. Growth rates for several values of the barotropic vorticity, q_B, for $m = 2$ and – – –, $\delta = 0.33$; ——, $\delta = 1.0$.

The region of instability for purely baroclinic vortices ($q_B = 0$) is illustrated in figure 2. For all δ, mode 2 is the first to become unstable as F_1 increases (broader vortices). Decreasing δ (increasing H_2) increases the critical value of $F_1 = F_{1c}$ for all m. In the limit $\delta \to 0$ we have the reduced gravity ($1\frac{1}{2}$-layer) model and the result that a circular vortex is linearly stable. In figure 3 the growth rates are shown. When δ is decreased the maximum growth rates are reduced. The net effect of an increasing lower layer depth is to stabilize the vortex.

Net barotropic circulation may be stabilizing or destabilizing. Stability regions for $m = 2$, $q_1 = 1$ and $\delta = 0.33$ and 1 are shown in figure 4. The corresponding growth rates for several values of q_B are plotted in figure 5. The choice of $q_1 = 1$ can be made without loss of generality and is equivalent to setting the velocity scale $U = L \times$ (dimensional value of q_1). Net barotropic flow introduces a maximum critical value of F_1. As q_B is increased above zero the vortex is stabilized and the growth rates are reduced. For $q_B \geqslant 1$ the vortex is stable to all modes since the vorticity is the same sign in both layers and heton formation is prohibited (or alternatively, since the radial vorticity gradient is the same sign everywhere in both layers the vortex must be stable, Pedlosky 1979). Thus, vorticity of opposite sign in the two layers is

a necessary condition for instability. For $q_B < 0$ the vortex is destabilized in the sense that the lower critical value of F_1 is reduced ($\delta < 1$) and the growth rates are increased. For very large negative q_B the region of instability becomes very small. In this limit the vortex is nearly completely barotropic and thus stable. Higher modes behave similarly and become unstable at successively larger F_1. Again, decreasing δ is stabilizing.

3. Contour dynamics formulation

Finite-amplitude evolution of unstable vortices can be studied using the contour dynamics method (Zabusky *et al.* 1979). Since the method has become quite standard, only an outline of the procedure and important steps for the two-layer formulation will be given. The formulation for the reduced-gravity ($1\frac{1}{2}$-layer) quasi-geostrophic system is discussed by Pratt & Stern (1986).

The contour dynamics method is based upon the presence of piecewise uniform potential vorticity in regions of space bounded by contours. Knowledge of the contours thus determines the potential vorticity distribution, which in turn allows solution for the flow field by inverting (2.1). For the system introduced in §2 conservation of potential vorticity in each layer gives

$$\nabla^2\psi_n + F_n(-1)^n(\psi_1-\psi_2) = \begin{cases} q_n & (\text{inside } C_n) \\ 0 & (\text{outside } C_n) \end{cases}, \tag{3.1}$$

where C_n is the contour which encloses the region (no longer necessarily circular) of uniform potential vorticity in each layer. Since the vorticity is uniform within the contours it is sufficient to follow the evolution of the contours. From (3.1) two equations for the barotropic,

$$\psi_B = \psi_1 + \delta^{-1}\psi_2, \tag{3.2a}$$

and baroclinic,

$$\psi_T = \psi_1 - \psi_2, \tag{3.2b}$$

modal components are,

$$\nabla^2\psi_B = q_B(x,y) = \begin{cases} q_1 & (\text{inside } C_1) \\ 0 & (\text{outside } C_1) \end{cases} + \delta^{-1}\begin{cases} q_2 & (\text{inside } C_2) \\ 0 & (\text{outside } C_2) \end{cases} \tag{3.3}$$

and

$$\nabla^2\psi_T - k^2\psi_T = q_T(x,y) = \begin{cases} q_1 & (\text{inside } C_1) \\ 0 & (\text{outside } C_1) \end{cases} - \begin{cases} q_2 & (\text{inside } C_2) \\ 0 & (\text{outside } C_2) \end{cases}, \tag{3.4}$$

where k is given by (2.4*c*).

The Green functions for the barotropic component, $(2\pi)^{-1}\log r$, and the baroclinic component, $-(2\pi)^{-1}K_0(kr)$, are used to construct the solutions to (3.3) and (3.4) at some point (x, y),

$$\psi_B(x,y) = (2\pi)^{-1}\int_{-\infty}^{\infty}\int_{-\infty}^{\infty} q_B(\xi,\eta)\log r\,\mathrm{d}\xi\,\mathrm{d}\eta, \tag{3.5a}$$

and

$$\psi_T(x,y) = -(2\pi)^{-1}\int_{-\infty}^{\infty}\int_{-\infty}^{\infty} q_T(\xi,\eta)\,K_0(kr)\,\mathrm{d}\xi\,\mathrm{d}\eta, \tag{3.5b}$$

where

$$r = [(x-\xi)^2 + (y-\eta)^2]^{\frac{1}{2}}.$$

The barotropic velocities (u_B, v_B) and baroclinic velocities (u_T, v_T) are found by taking $(-\partial/\partial y, \partial/\partial x)$ of (3.5*a*, *b*). Since the vorticity is uniform within each contour and zero outside, the divergence theorem is used to convert the resulting area integrals into contour integrals

$$\begin{pmatrix} u_B(x,y) \\ v_B(x,y) \end{pmatrix} = \frac{-q_1}{2\pi} \oint_{C_1} \log r \begin{pmatrix} d\xi \\ d\eta \end{pmatrix} - \delta^{-1} \frac{q_2}{2\pi} \oint_{C_2} \log r \begin{pmatrix} d\xi \\ d\eta \end{pmatrix}, \tag{3.6a}$$

and

$$\begin{pmatrix} u_T(x,y) \\ v_T(x,y) \end{pmatrix} = \frac{q_1}{2\pi} \oint_{C_1} K_0(kr) \begin{pmatrix} d\xi \\ d\eta \end{pmatrix} - \frac{q_2}{2\pi} \oint_{C_2} K_0(kr) \begin{pmatrix} d\xi \\ d\eta \end{pmatrix}. \tag{3.6b}$$

From (3.2) and (3.6) the velocities in each layer (u_n, v_n) can be reconstructed as

$$\begin{pmatrix} u_n(x,y) \\ v_n(x,y) \end{pmatrix} = \frac{\delta}{2\pi(1+\delta)} \sum_{l=1,2} \oint_{C_l} [a_{n,l} \log r + b_{n,l} K_0(kr)] \begin{pmatrix} d\xi \\ d\eta \end{pmatrix}, \tag{3.7}$$

where

$$\begin{bmatrix} a_{1,1} & a_{1,2} \\ a_{2,1} & a_{2,2} \end{bmatrix} = \begin{bmatrix} -q_1 & -\delta^{-1}q_2 \\ -q_1 & -\delta^{-1}q_2 \end{bmatrix},$$

and

$$\begin{bmatrix} b_{1,1} & b_{1,2} \\ b_{2,1} & b_{2,2} \end{bmatrix} = \begin{bmatrix} \delta^{-1}q_1 & -\delta^{-1}q_2 \\ -q_1 & q_2 \end{bmatrix}.$$

In (3.6) and (3.7) the sense of the contour integrals is counterclockwise. If the contours are defined by node points $(x_i, y_i)_n$ then the temporal evolution of C_n can be found from the Lagrangian advection of each node point according to

$$\frac{d}{dt} \begin{pmatrix} x_i \\ y_i \end{pmatrix}_n = \begin{pmatrix} u_n(x_i, y_i) \\ v_n(x_i, y_i) \end{pmatrix}, \tag{3.8}$$

where the velocities (u_n, v_n) are given by (3.7).

Note that the method may be generalized to n layers ($n > 2$) by extending the modal decomposition (3.2), then repeating the subsequent development. This leads to an equation for the velocities similar to (3.7), but including contributions from all the contours and modal components.

Following Pratt & Stern (1986) the velocities are found by using the trapezoidal rule to compute the contour integrals in (3.7). The temporal integration of (3.8) is accomplished using either a second-order Runge–Kutta method or the second-order Adams–Bashforth explicit multi-step method (Dahlquist & Björck 1974). The Adams–Bashforth method requires only one computation of the right-hand side of (3.8) per timestep, as opposed to two computations for the Runge–Kutta method and thus was used for most of the results presented below. Comparisons of the methods gave indistinguishable results at sufficiently small timesteps. Further savings in computational effort may be realized using symmetries of the problem when $q_B = 0$, $\delta = 1$. If the initial condition is a single normal-mode (see §4), one contour is an inverted image of the other so that only one contour needs to solved for explicitly. Angular symmetry is also present and only N/m points need to be tracked.

Most of the runs discussed below used 50 node points for each contour and a timestep of $\Delta t = 0.15$. Conservation of vorticity requires that the area within each contour remain constant. In all runs the areas remained within 1–2% of the initial area unless the node points became excessively bunched and a contour crossed over itself. At this time the numerical solution became unstable and the subsequent data was disregarded. Node adjustment or regularization procedures (Zabusky &

Overman 1983) were not employed. Test runs with high resolution of 100–200 points per layer showed some quantitative differences in details at large times, but the qualitative features at these times remained.

4. Numerical results

In this section the finite-amplitude evolution of circular vortices is examined. The contour shape of the initial condition is given by $r_n = 1+\eta_n$ where

$$\eta_n = \mathrm{Re}\{D_n \mathrm{e}^{\mathrm{i}(m\theta-\omega t)}\} = \mathrm{Re}\{|D_n| \mathrm{e}^{\mathrm{i}(m\theta-\omega t+\beta_n)}\}. \tag{4.1}$$

Here η_n is the perturbation in layer n, D_n is the complex amplitude and β_n is the phase shift. The perturbations used are the growing normal-mode solutions (2.8) of the linear stability problem. The contour shape η_n is related to the flow field $\Psi_n+\phi_n$ by the linearized kinematic boundary condition at $r = 1$,

$$\left(\frac{\partial}{\partial t}+\frac{V_n}{r}\frac{\partial}{\partial\theta}\right)\eta_n = \frac{-1}{r}\frac{\partial\phi_n}{\partial\theta}. \tag{4.2}$$

This determines D_n as

$$D_n = \frac{A(1+(-\delta)^{n-1}(B/A))}{V_n(1)-c}, \tag{4.3}$$

where A is an arbitrary real constant, B/A is found from (2.10), $V_n(r)$ is found from (2.5) and c is given by (2.11). Initial disturbance amplitudes, $|D_n|$, considered were in the range $[0.01, 0.1]$. Some runs were made with arbitrary amplitudes and phases and so do not correspond to normal modes. As in §2 we set $q_1 = 1$ without loss of generality. The focus will be on vortices with equal layer depths ($\delta = 1$). The behaviour with $\delta \neq 1$ is quantitatively, but not qualitatively different.

4.1. *Supercritical evolution: explosive behaviour*

Consider first the evolution of vortices with zero net barotropic circulation, $q_B = 0$, equal layer depths, $\delta = 1$, and supercriticality $\Delta \equiv (F_1-F_{1c})/F_{1c} = O(1)$. An example of the typical unstable finite-amplitude evolution for an $m = 2$ normal-mode disturbance is shown in figure 6(*a*). The initial perturbations of the cyclonic upper layer pair with the nearest perturbations in the anticyclonic lower layer. Each pair propagates outward by self-advection leading to splitting of the original vortex. Thin filaments connect the separated eddies in each layer. Because the model is conservative these filaments will continue to elongate as the vortex pairs move apart. Presumably, in a non-conservative system viscosity would eventually cause the filaments to break. We have not made any attempt to cut the filaments since their presence does not appear to influence the main features of the evolution, namely the pairing and subsequent break up of the initial vortex. Figure 6(*a*) qualitatively corresponds to figure 5 ($\lambda = 1.0$) in Hogg & Stommel (1985*a*) where an unstable cloud of point vortices evolves to form two composite hetons.

The splitting in figure 6(*a*) occurs rapidly. After 1–2 circulation periods two distinct pairs have formed. Shown in figure 6(*b*) is the evolution of the amplitudes of wavenumbers 2 and 4 found from Fourier analysis of the data in figure 6(*a*). Initially wavenumber 2 grows at the linear rate. Later, nonlinear interaction generates mode 4 and the vortex subsequently splits.

The finite-amplitude evolution of unstable vortices is not sensitive to the initial

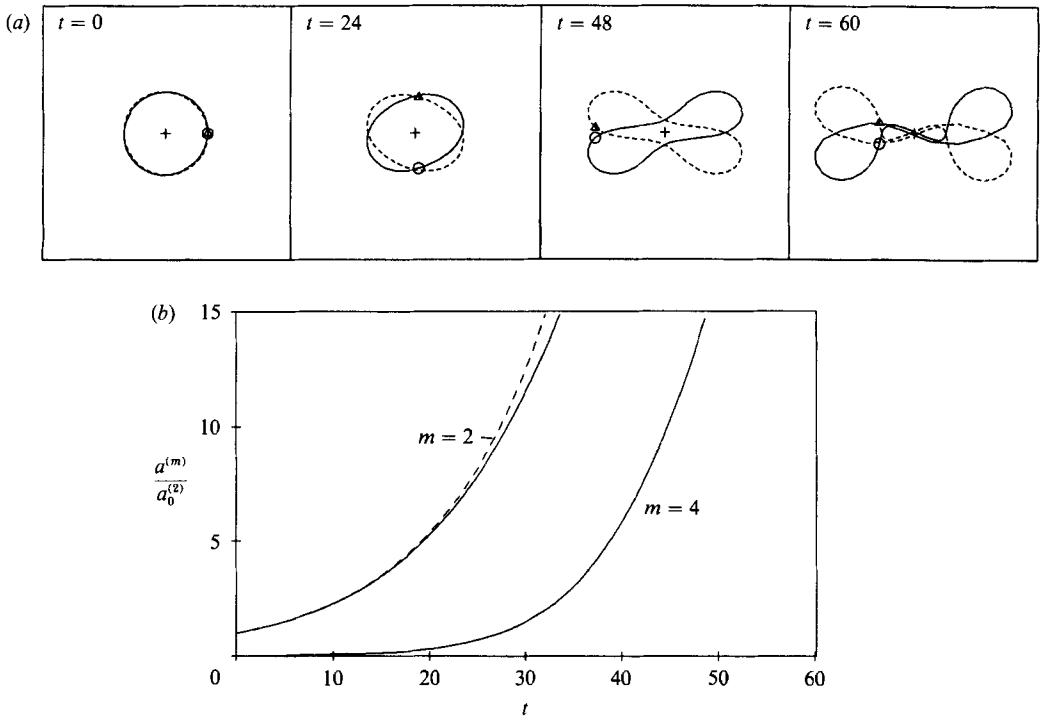

FIGURE 6 (*a*) Evolution of an unstable vortex with an $m = 2$ normal-mode perturbation. $(F_1, \delta, q_1, q_2, |D_n|) = (2.5, 1, 1, -1, 0.025)$. In this and subsequent contour figures: ——, the upper layer contour; – – –, the lower layer contour; ○, node point 1 in the upper layer; △, node point 1 in the lower layer. (*b*) Growth of the Fourier amplitude $a^{(m)}$ (normalized by the initial perturbation amplitude $a_0^{(2)}$) *vs.* time for ——, the run in (*a*) and – – –, the linear theory.

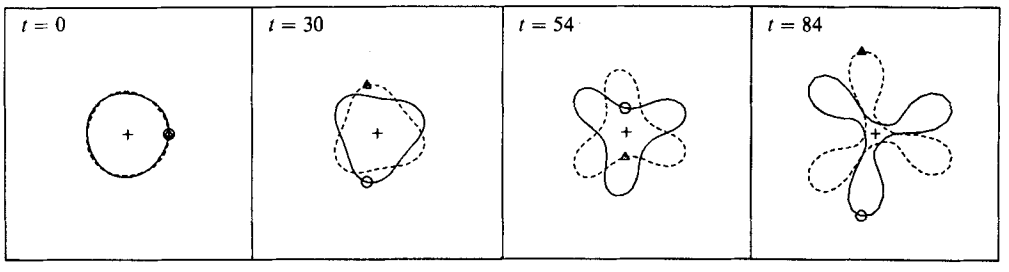

FIGURE 7. Evolution of an unstable vortex with an $m = 3$ normal-mode perturbation. $(F_1, \delta, q_1, q_2, |D_n|) = (5.0, 1, 1, -1, 0.025)$.

amplitude of the disturbance, though the splitting occurs sooner as the amplitude of the disturbance is increased. The initial growth rate does not depart significantly from the linear theory for $|D_n| \leqslant 0.1$.

Figure 7 shows a run in the regime when $m = 3$ is unstable. Mode 2 is also linearly unstable but the initial condition contained only mode 3. Examples with several unstable modes in the initial condition will be discussed in §4.4. The evolution is similar to figure 6, with three offset pairs forming. Additionally, a baroclinic vortex is left in the centre. Again the initial growth is at the linear rate.

Pairing of perturbations of opposite signs is characteristic of all unstable vortices,

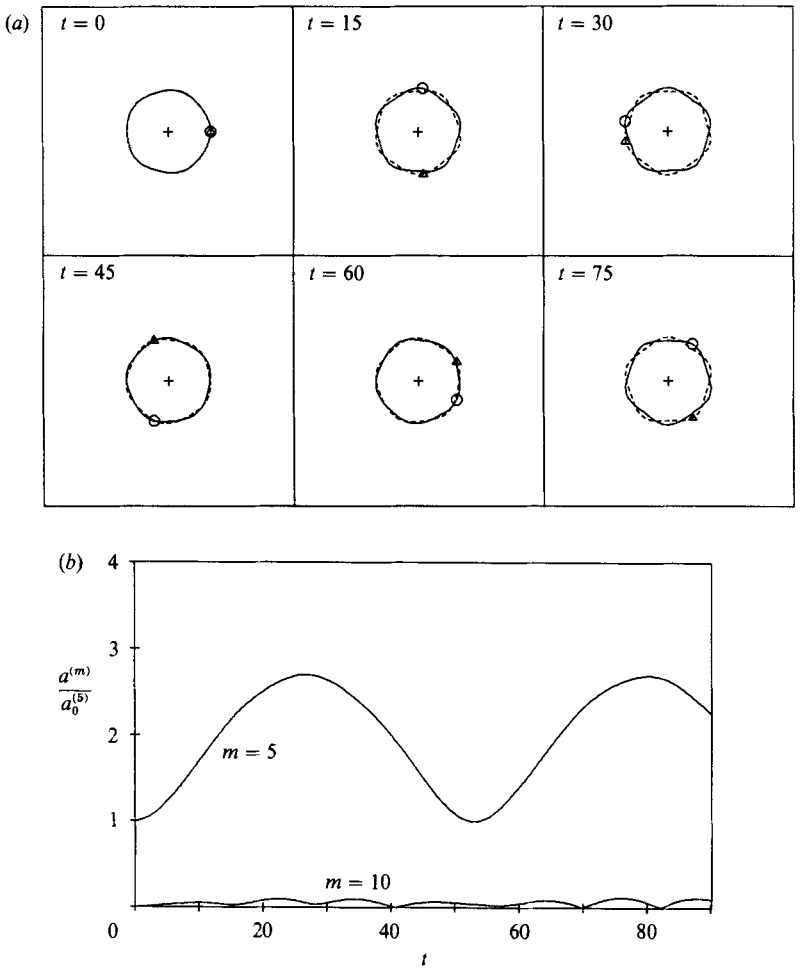

FIGURE 8. (*a*) Vacillation of weakly supercritical $m = 5$ perturbation. $(F_1, \delta, q_1, q_2, |D_n|, \beta_n) = (12.5, 1, 1, -1, 0.02, 0)$. (*b*) Fourier amplitudes for $m = 5$ and 10 for the experiment in (*a*).

with the number of pairs equal to the perturbed mode. For $m \geqslant 3$ a vortex is left at the centre. If the initial disturbance does not have the correct phase β_n for a growing normal mode, but is an unstable wavenumber, the vortex is still unstable. This follows because the initial condition can be decomposed into a superposition of a growing and a decaying normal mode. Thus the finite-amplitude state is qualitatively the same as the corresponding growing normal-mode case.

4.2. *Supercritical evolution: vacillation*

The unstable runs examined above were all highly supercritical with $\Delta = O(1)$. Pedlosky (1985) analysed the weakly nonlinear ($\Delta \ll 1$) evolution of a straight cloud band and showed that all linearly unstable wavenumbers were explosively unstable (i.e. no vacillation). Finite, but small, perturbations of initial states just into the stable regime could also be explosively unstable if the initial disturbance was large enough. However, our numerical study does not behave according to this weakly nonlinear theory. Numerical experiments with one unstable wavenumber show a regime in which supercritical conditions lead to amplitude vacillation. This finding

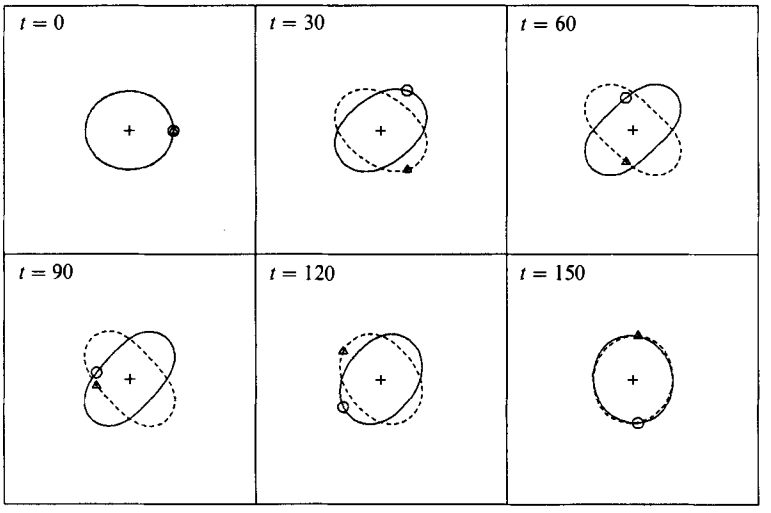

FIGURE 9. Large-amplitude vacillation of a weakly supercritical $m = 2$ perturbation. $(F_1, \delta, q_1, q_2, |D_n|, \beta_n) = (1.5, 1, 1, -1, 0.05, 0)$.

is confirmed by Flierl (1988) and discussed further in §5. Figure 8(*a*) shows an example with $m = 5$. The amplitude of mode 5 settles into a long period oscillation as shown in figure 8(*b*). The maximum amplitude of the vacillating mode slowly decays with time. This decay is consistent with reduction in the area invariant (potential vorticity) and appears to be due to numerical error over long integration times. For a given wavenumber the oscillation period and the maximum amplitude increase as the supercriticality is increased. Large-amplitude oscillations are illustrated in figure 9 where an $m = 2$ perturbation grows very large, outside the range of applicability of weakly nonlinear analysis. Slightly subcritical vortices remain stable even for large initial disturbances ($|D_n| \leqslant 0.1$). The evolution is similar to the weakly supercritical cases discussed above.

Vacillating behaviour is found for all wavenumbers. In figure 10 we show the location of the boundary between the vacillating and explosive regime for $q_B = 0$ and $\delta = 1$. The location of the boundary is not sensitive to the initial phase relation (i.e. normal-mode structure) or to amplitude for $|D_n| \leqslant 0.1$, although the maximum amplitudes do depend on the initial phases. The range of vacillating behaviour decreases with decreasing m, but is still present for $m = 2$. The boundary is sensitive to the number of node points used to define the contour. For more than approximately $50m$ points per layer the boundary is stable, but the vacillation range increases as the number of points decreases below this value. The data used to construct figure 10 used sufficient numbers of points to achieve a stable boundary.

The qualitative behaviour of vortices with unequal layer depths $\delta \neq 1$ and $q_B = 0$ is the same for $\delta = 1$. Explosive growth and vacillation regimes occur though we have not documented the ranges.

4.3. *Net barotropic circulation*

An example of an unstable case with a net barotropic flow ($q_B \neq 0$) is illustrated in figure 11 for an $m = 2$ disturbance. The symmetry between layers found when $q_B = 0$ is lost. The tendency for elongation and pairing remains; however, the layer with vorticity of sign opposite to q_B splits first. The development of distinct heton pairs

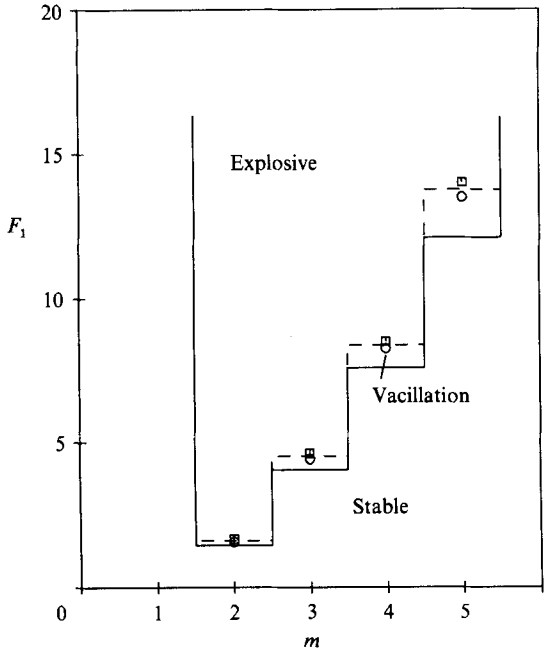

FIGURE 10. Stability diagram for $(q_B, \delta) = (0, 1)$ showing – – –, the transition from vacillation to explosive growth. The symbols correspond to numerical experiments which showed ○, vacillation or □, explosive instability. ——, linear stability boundary.

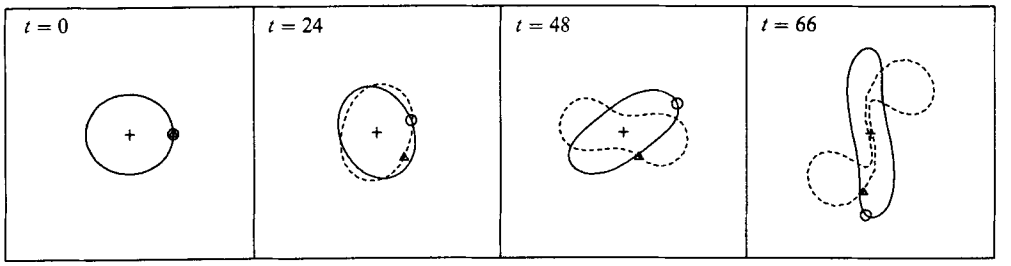

FIGURE 11. Unstable evolution of a vortex with net barotropic flow $q_B = 0.5$ for an $m = 2$ perturbation. $(F_1, \delta, q_1, q_2, m, |D_n|, \beta_n) = (2.5, 1, 1, -0.5, 2, 0.05, 0)$.

is retarded as the barotropic flow is increased. Figure 12 illustrates this behaviour for an $m = 3$ instability. In figure 12(*a*), $q_B = 0.1$ and asymmetrical pairs emerge. For $q_B = 0.5$ (figure 12*b*) the weaker layer is split into 3 vortices and a remaining central core. The stronger upper layer is distorted but remains intact except for the ejection of filaments. The filaments are stretched by interaction with both the vortices in the opposite layer and the vortex core in the same layer. When $q_B = 0.75$ (figure 12*c*) no filaments are present at a comparable time. The tendency for the layer with vorticity the same sign as q_B to remain intact increases as the strength of the barotropic circulation increases. The vorticity in the other layer may act to cause detrainment, but is not strong enough to result in heton development.

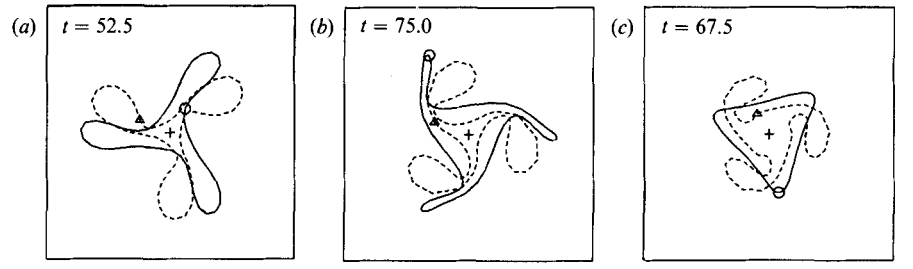

FIGURE 12. Large-time states for experiments with net barotropic circulation and $m = 3$ perturbations. $(F_1, \delta, m, |D_n|, \beta_n) = (7.0, 1.0, 3, 0.05, 0)$. (*a*) $q_B = 0.1$; (*b*) $q_B = 0.5$; (*c*) $q_B = 0.75$.

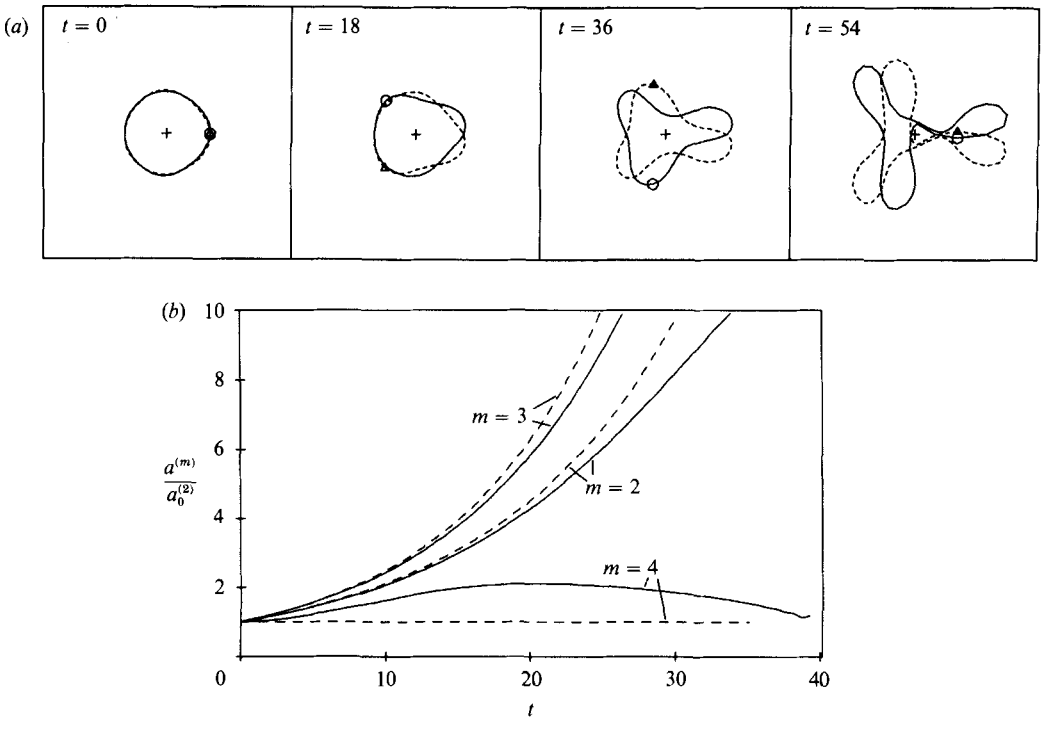

FIGURE 13. (*a*) Evolution of unstable vortex with a superposition of $m = 2$, 3 and 4 normal-modes initial condition for $F_1 = 7.0$. $(\delta, q_B, |D_n^{(m)}|) = (1.0, 0, 0.02)$. (*b*) Fourier amplitudes for ——, $m = 2$, 3 and 4 and – – –, the linear theory.

4.4. *Multiple wavenumber disturbances*

When more than one wavenumber is unstable the interaction of the growing modes is of interest. To examine this issue experiments with initial conditions consisting of the superposition of growing normal-modes 2, 3 and 4 with equal amplitudes were conducted for the purely baroclinic vortex $q_B = 0$ with $\delta = 1$. The results show that the wavenumber with the largest linear growth rate will dominate at finite amplitude. An example for $F_1 = 7.0$ is shown in figure 13. Mode 3 has the largest growth rate ($\omega_i^{(2)} = 0.0760$, $\omega_i^{(3)} = 0.0926$ and $\omega_i^{(4)} = 0$) and three distorted heton pairs are formed. From the evolution of the Fourier amplitudes (figure 13*b*) the unstable modes initially grow at their linear rates with little evidence of strong interaction

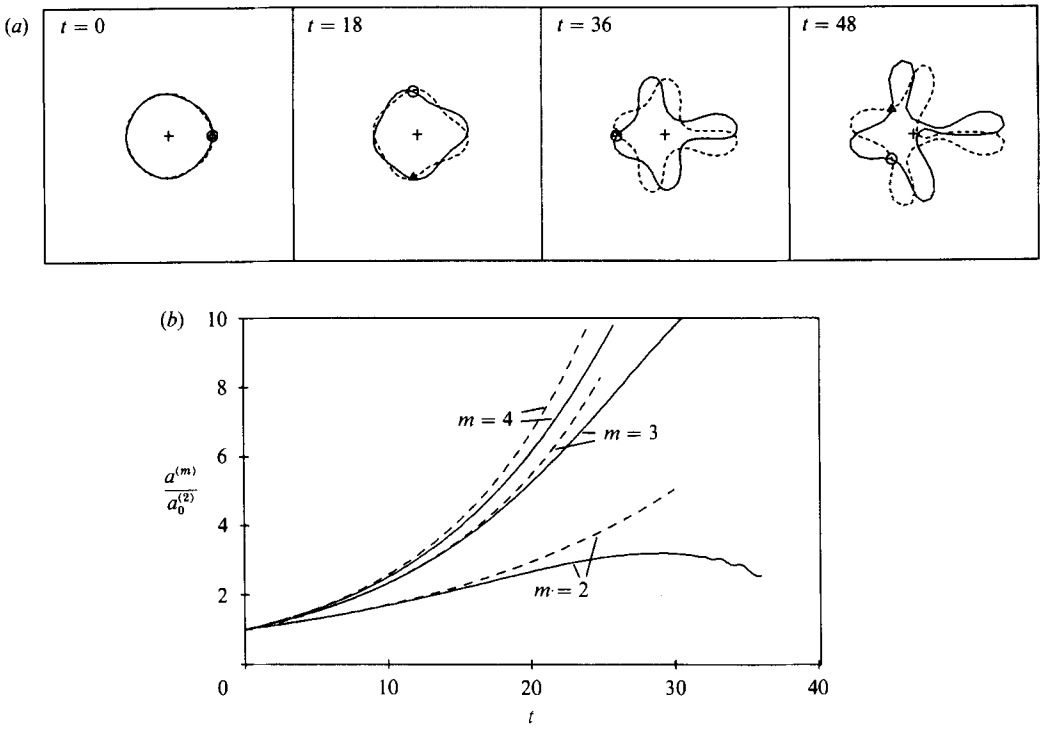

FIGURE 14. Same as figure 13 except with $F_1 = 14.0$.

before the vortex splits. Figure 14 shows another example at $F_1 = 14.0$ where mode 4 has the largest linear growth rate ($\omega_i^{(2)} = 0.0542$, $\omega_i^{13)} = 0.0854$ and $\omega_i^{(4)} = 0.0955$). The final state is again consistent with the linear theory. These conclusions do not require normal-mode phase structure in the initial conditions. Owing to the explosive nature of the instability, differences in the initial amplitudes of the modes may be important. The mode with the largest linear growth rate may not dominate if its initial amplitude is much smaller than the amplitude of any other growing mode. The slower growing mode may reach a large amplitude and destroy the original vortex before the fastest growing mode becomes significant.

5. Discussion

This study of the stability and finite-amplitude behaviour of circular baroclinic vortices has demonstrated that the continuous model contains similar behaviour to the point vortex model (Hogg & Stommel 1985*a*). The main feature of an explosively unstable vortex is the pairing of vorticity perturbations of opposite signs in opposite layers at the cloud boundary. These pairs interact to form continuous hetons and the vortex is split as the pairs propagate outward. Even though both δ and q_B are parameters of the problem, q_B is the most important one governing the finite-amplitude evolution of unstable vortices. For vortices with sufficient net barotropic circulation the generation of hetons at the cloud boundaries may not occur. The layer with vorticity of the same sign as the net barotropic flow will emit filaments, but remain mostly intact. Thus spreading of fluid (and heat) is inhibited since the lateral transport mechanism, hetons, is no longer present.

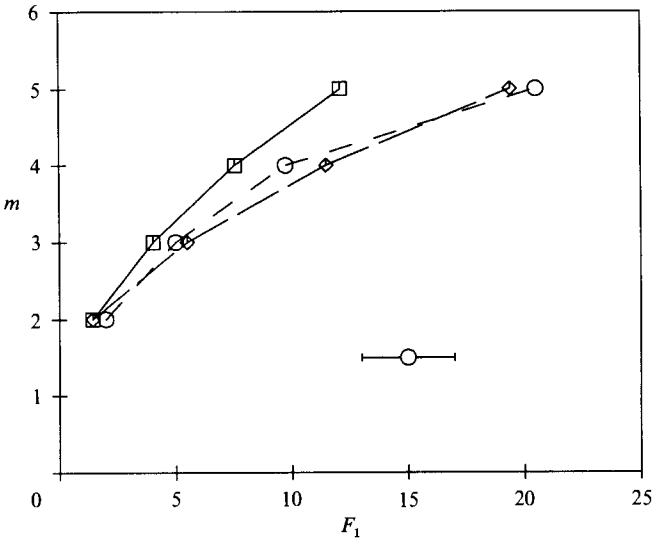

FIGURE 15. Transitions between modes of instability as a function of F_1 from ○, the experiments of Griffiths & Linden (1981), and ◇, from the linear theory ($\delta = 1$, $q_B = 0$) based on the mode with the largest growth rate. Also shown is □, the linear stability boundary.

One feature which does not appear in the weakly nonlinear theoretical analysis of Pedlosky (1985) is the occurrence of vacillation for weakly supercritical conditions. Flierl (1988) uses an analytic theory which employs the contour dynamical procedure (i.e. exploits the linearity of the relationship between the potential vorticity and the streamfunctions) and also finds vacillation for both the straight cloud band (the only case considered by Pedlosky) and the circular heton cloud. Thus the geometry does not appear to be the controlling factor. The difference between the new studies and Pedlosky lies in the determination of the streamfunctions in the small region between η_1 and η_2. Pedlosky's approach leads to an error which is avoided here. The reader is referred to Flierl for a more complete discussion. Though the differences are small, the final result is sensitive because it is the details of the interactions of the frontal perturbations which determine the evolution. Unlike Flierl, our numerical calculations show that the vacillation regime is limited to small supercriticalities, a result not obtained with the weakly nonlinear theory.

Hogg & Stommel (1985*a*) found that when six hetons were spaced equally around a circle they would not explode if the ratio of the circle radius to the deformation radius was not too large. Individual vortices would move around the vortex along undulating paths. This behaviour is similar to the vacillation found here. A circle of hetons has the velocity shear concentrated at the circle rim as would a broad continuous heton cloud. The vacillation also appears to be analogous to the reformation of weakly supercritical vortices with a continually varying, rather than piecewise uniform, distribution of potential vorticity studied by Ikeda (1981). However, his calculations were not carried very far in time, so we cannot be sure that the return to a circular eddy is the decay stage of a vacillation cycle or the end state.

When more than one unstable wavenumber is present in the initial condition the wavenumber with the largest linear growth rate will dominate at large times. The individual modes grow at approximately their linear rates with little interaction prior to break up of the vortex. In contrast, studies of baroclinic instability in two-

layer zonal flows (Eady-type models) demonstrate that the linearly most unstable wavenumber will not dominate at finite amplitude (Pedlosky 1981; Hart 1981; Klein & Pedlosky 1986). The difference in behaviour is probably due to the explosive nature of the instability in the present study. At least one of the initial wavenumbers will not vacillate and the basic state vortex will eventually be destroyed. In the channel models equilibration or vacillation is the general rule. Alteration of the mean state by the fastest growing wavenumber permits a different (lower) wavenumber to eventually dominate and equilibrate.

Griffiths & Linden (1981) conducted laboratory experiments on the stability of two-layer baroclinic vortices formed by the release of a cylindrical volume of buoyant fluid in a rotating system. Though the eddies generated by this technique had an interface which intersected the free surface, and thus were ageostrophic, the behaviour of unstable vortices was very similar to the calculations shown above. Griffiths & Linden (1981) emphasized the importance of interaction of vorticity of opposite signs in the break up. Their cartoon of an observed $m = 3$ instability (figure 6, Griffiths & Linden 1981) bears a remarkable resemblance to our figure 7. In figure 15 we have plotted the transition points for observed modes of instability from their experiments (figure 5 in Griffiths & Linden) for vortices with an initial depth of half the total depth which corresponds to $\delta = 1.0$ in the present model. We have taken F_1 to equal their $\theta_0^{-1} = f^2 L_0^2 / g' H_0$ where L_0 and H_0 are respectively the radius and depth of the initial cylindrical volume. Also shown are the transition points based on the fastest growing mode from the linear theory with $\delta = 1$ and $q_B = 0$. The agreement is quite good. Certainly ageostrophic effects are important, but the model captures the basic features.

The authors wish to thank Glen Flierl and Lorenzo Polvani for helpful discussions and for sharing their unpublished results on related work. This work was supported by grants from the National Science Foundation (OCE 96-14842) and the Office of Naval Research (N00014-87-K-0007). Woods Hole Oceanographic Institution Contribution Number 6673.

REFERENCES

DAHLQUIST, G. & BJÖRCK, Å, 1974 *Numerical Methods*. Prentice-Hall.

FLIERL, G. R. 1988 On the instability of geostrophic vortices. *J. Fluid Mech.* **197**, 349–388.

GRIFFITHS, R. W. & LINDEN, P. F. 1981 The stability of vortices in a rotating, stratified fluid. *J. Fluid Mech.* **105**, 283–316.

HART, J. E. 1981 Wavenumber selection in nonlinear baroclinic instability. *J. Atmos. Sci.* **38**, 400–408.

HOGG, N. G. & STOMMEL, H. M. 1985*a* Hetonic explosions: The breakup and spread of warm pools as explained by baroclinic point vortices. *J. Atmos. Sci.* **42**, 1465–1476.

HOGG, N. G. & STOMMEL, H. M. 1985*b* The heton, an elementary interaction between discrete baroclinic geostrophic vortices, and its implications concerning eddy heat-flow. *Proc. R. Soc. Lond.* A **397**, 1–20.

IKEDA, M. 1981 Instability and splitting of mesoscale rings using a two layer quasi-geostrophic model on an f-plane. *J. Phys Oceanogr.* **11**, 987–998.

KLEIN, P. & PEDLOSKY, J. 1986 A numerical study of baroclinic instability at large supercriticality. *J. Atmos. Sci.* **43**, 1243–1262.

KOZLOV, V. F., MAKAROV, V. G. & SOKOLOVSKIY, M. A. 1986 Numerical model of baroclinic instability of axially symmetric eddies in a two-layer ocean. *Izv. Akad. Nauk, SSSR Atmos. Ocean. Phys.* **22**, 674–678.

PEDLOSKY, J. 1979 *Geophysical Fluid Dynamics*. Springer.

PEDLOSKY, J. 1981 The nonlinear dynamics of baroclinic wave ensembles. *J. Fluid Mech.* **102**, 169–209.

PEDLOSKY, J. 1985 The instability of continuous heton clouds. *J. Atmos. Sci.* **42**, 1477–1486.

PRATT, L. J. & STERN, M. E. 1986 Dynamics of potential vorticity fronts and eddy detachment. *J. Phys. Oceanogr.* **16**, 1101–1120.

YOUNG, W. R. 1985 Some interactions between small numbers of baroclinic, geostrophic vortices. *Geophys. Astrophys. Fluid Dyn.* **33**, 35–62.

ZABUSKY, N. J., HUGHES, M. & ROBERTS, K. V. 1979 Contour dynamics for the Euler equations in two dimensions. *J. Comp. Phys.* **30**, 96–106.

ZABUSKY, N. J. & OVERMAN, E. A. 1983 Regularization of contour dynamical algorythms. 1. Tangential regularization. *J. Comp. Phys.* **52**, 351–373.